



LJMU Research Online

Qiu, Z, Qiu, Y, Demore, CEM and Cochran, S

Implementation of a PMN-PT piezocrystal-based focused array with geodesic faceted structure

<http://researchonline.ljmu.ac.uk/id/eprint/9059/>

Article

Citation (please note it is advisable to refer to the publisher's version if you intend to cite from this work)

Qiu, Z, Qiu, Y, Demore, CEM and Cochran, S (2016) Implementation of a PMN-PT piezocrystal-based focused array with geodesic faceted structure. Ultrasonics, 69. pp. 137-143. ISSN 0041-624X

LJMU has developed **LJMU Research Online** for users to access the research output of the University more effectively. Copyright © and Moral Rights for the papers on this site are retained by the individual authors and/or other copyright owners. Users may download and/or print one copy of any article(s) in LJMU Research Online to facilitate their private study or for non-commercial research. You may not engage in further distribution of the material or use it for any profit-making activities or any commercial gain.

The version presented here may differ from the published version or from the version of the record. Please see the repository URL above for details on accessing the published version and note that access may require a subscription.

For more information please contact researchonline@ljmu.ac.uk

<http://researchonline.ljmu.ac.uk/>

33 movement in the focal point is necessary, fewer elements and simpler time delays are needed, reducing the
34 complexity of the driving circuitry.

35 Historically, piezoceramics have been the most commonly used materials in ultrasound transducer arrays
36 but, recently, the improved performance offered by relaxor-based piezocrystals in the $\text{Pb}(\text{Mg}_{1/3}\text{Nb}_{2/3})\text{O}_3$ -
37 PbTiO_3 (PMN-PT) family has been recognized. Piezocrystals are now used widely in biomedical ultrasound
38 imaging and investigation of their possibilities is under way in nondestructive evaluation, particle
39 manipulation and underwater sonar [7-10] based on piezoelectric properties including $k_{33} \approx 90\%$ and
40 $d_{33} > 1500$ pC/N [11]. Bulk, monolithic piezocrystal has little advantage over piezoceramic, with the values of
41 k_t being similar, but improved performance can be realized in configurations such as the planks used in
42 biomedical imaging arrays and the pillars used in piezocomposites.

43 PMN-PT itself, termed a Generation I material, is susceptible to changes in functional properties at
44 elevated temperature and pressure [12], but Generations II and III, respectively exemplified by ternary PIN-
45 PMN-PT and doped ternary Mn:PIN-PMN-PT, are under development to reduce these effects whilst
46 maintaining much of the performance advantage over piezoceramic, e.g. in terms of k_{33} and d_{33} that determine
47 piezocomposite performance. Piezocrystal composites thus have potential to improve the effectiveness of
48 focused ultrasound transducers and the work reported here contributes to this by describing the fabrication and
49 testing of a 2D concave phased array made with Generation I piezocrystal.

50 A widely-reported method to fabricate concave transducer arrays is to place individual single-element
51 transducers in a prefabricated frame at predetermined positions [6, 13]. This requires manufacture of each
52 individual array element separately and the presence of the frame can significantly reduce the array fill-factor,
53 i.e. the percentage surface coverage of the active piezoelectric material, and thus the focusing gain and
54 acoustic energy output of the transducer. As an alternative, Raju et al. [14] proposed an array design using a
55 spherically-focused ceramic bowl with printed electrodes defining the elements. However, fabrication of
56 curved sections from piezocrystal boules would be wasteful of material which costs $\$0.5 - 3 / \text{mm}^3$, and more
57 importantly, performance would be decreased by the lack of alignment between the piezocrystal axes and the
58 surface of the array. Mechanical forming to focus piezocrystal transducers has been achieved successfully
59 using mechanical hard-press [15] and dimpling techniques [16], but reports are limited to single-element
60 transducers. Other possibilities are to thermally form a 1-3 connectivity piezoelectric - polymer composite into
61 the desired shape [17] or to use flexible polymers for flexible composites [18], but these may be difficult at the

62 frequencies of interest here, below 1.0 MHz, and the values of volume fraction, e.g. $VF > 50\%$, used in
63 focused ultrasound applications.

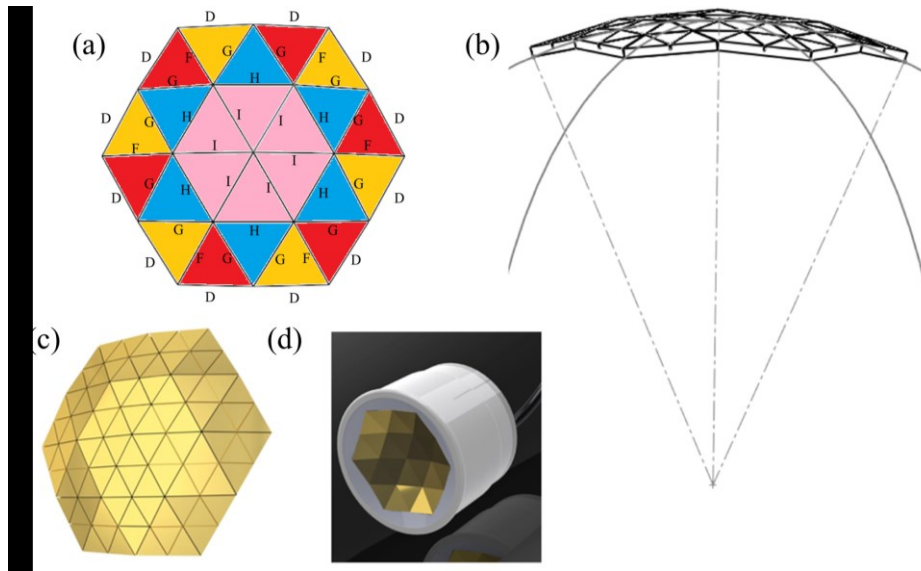
64 In this short communication, a novel array structure is described to utilize 1-3 connectivity piezocrystal -
65 polymer composites in a geometrically focused array transducer. The practical challenges associated with the
66 fabrication of the array structure and electrical interconnects to the elements are addressed. 3D printing is
67 introduced to aid assembly. The performance of the array is demonstrated and its use with a 32-channel
68 modular array controller is described, illustrating both beam shaping and the relocation of the focus required
69 in focused ultrasound applications.

70 **2. Geodesic Structure**

71 The faceted spherical structure proposed in this work is drawn from the architectural design of geodesic
72 domes. These domes comprise multiple triangles approximately equal in size, with their vertices lying on the
73 surface of a sphere. The planes of the triangles lie physically inside the sphere but the structure approximates a
74 sphere whilst maximizing the coverage of the aperture with the piezoelectric material.

75 A section of an icosahedron dome structure with dome frequency $6V$, referring to a structure with six
76 subdivisions of the original triangles in one icosahedron [19], was chosen for the proposed array. In total, the
77 section requires 24 triangular flat plates positioned as shown in Fig. 1. To match a commercial piezoelectric
78 bowl used as a reference, the target operating frequency of the array was 1.0 MHz and its aperture was 62 mm
79 across its largest diagonal, with a natural focal distance of 75 mm, equal to the dome radius, giving $f\# \approx 1.2$.
80 Table 1 lists the four triangular geometries in this design, with their side lengths and corresponding angles.
81 Each triangle is named for its sides taken in a clockwise direction. Five side lengths in total are needed,
82 denoted D, F, G, H and I. Triangles HGG and HII are isosceles and triangles DFG and DGF are scalene; six of
83 each type are required. These triangles were machined by a precision dicing saw (MicroAce 66, Loadpoint
84 Ltd., Wiltshire, UK) with dicing position accuracy of 0.001 mm and theta axis resolution of 0.0005°.

85 To increase the number of array elements for more flexible control over beam forming, each triangular
86 plate was sub-divided into four smaller triangular elements by dicing along the mid-segments of the plates to
87 half their thickness. The number of individual transducer elements was thus increased from 24 to 96, as shown
88 in Fig. 1c, with only one additional step in the fabrication process. Each sub-diced element is connected to an
89 individual signal wire at the rear and a common silver ink electrode ground with a single wire at the front.



90

91 *Figure 1. Illustration of geodesic array transducer. (a) Configuration of 24 triangular plates with four different shapes;*
 92 *(b) overall array configuration with geometrical focus; (c) rear view of the array with 96 sub-diced individual elements;*
 93 *(d) computer-aided design front view of the array assembly.*

Table 1. Side lengths and corresponding angles of the four triangular plate designs

Geometries	L_1 (mm)	L_2 (mm)	L_3 (mm)	α_1 (Degree)	α_2 (Degree)	α_3 (Degree)	
Triangle-DFG	15.21	14.85	15.44	60.25	61.80	57.95	
Triangle-DGF	15.21	15.44	14.85	60.25	57.95	61.80	
Triangle-HGG	16.15	15.44	15.44	63.06	58.47	58.47	
Triangle-HII	16.15	16.24	16.24	59.64	60.18	60.18	

* L_i ($i = 1, 2, 3$) are the side lengths of triangles where i refers to the 1st, 2nd, and 3rd letters respectively of the triangles' names.

94

95 **3. Piezomaterials**

96 The geodesic faceted structure was realized with two different piezoelectric materials: bulk ceramic to test
 97 the fabrication process and geodesic geometry and 1-3 connectivity PMN-PT piezocrystal – epoxy composite
 98 for performance evaluation. As noted previously, 1-3 composite is necessary to take advantage of the high
 99 values of k_{33} and d_{33} of PMN-PT.

100 For initial evaluation of fabrication, a pre-electroded piezoceramic plate, thickness 2 mm for 1 MHz
 101 operational frequency, (PZ26, Meggitt Sensor Systems, Kvistgaard, Denmark) was diced and separated into
 102 24 triangular plates and then sub-diced into 96 sub-elements with 210 μm kerf width and 1 mm depth.
 103 Similarly, another set of 24 triangular plates was diced from 1-3 connectivity PMN-29%PT (Sinoceramic Inc.,
 104 Shanghai, China) - hard polymer (Epofix, Struers A/S, Ballerup, Denmark) piezocomposite fabricated in
 105 house using the dice-and-fill method. Epofix was chosen for its low shrinkage, mechanical strength, low
 106 Poisson's ratio, and chemical resistance [20]. The piezocomposite material had a dicing kerf of 113 μm , a
 107 volume fraction, $VF = 60\%$, and a pillar aspect ratio (width to thickness), $PAR = 0.32$. It was lapped to a

108 thickness of 1.2 ± 0.02 mm to achieve the 1.0 MHz operational frequency. Electrodes were applied on both
109 sides of the triangular piezocomposite plates using silver ink (118-09A/B, Creative Materials Incorporated,
110 USA) cured at 65°C for 16 h. One electrode face on each triangular piezocomposite plate was part-diced into
111 four smaller triangular divisions, while the ground electrodes on the opposite faces were left intact.

112 **4. Array Assembly**

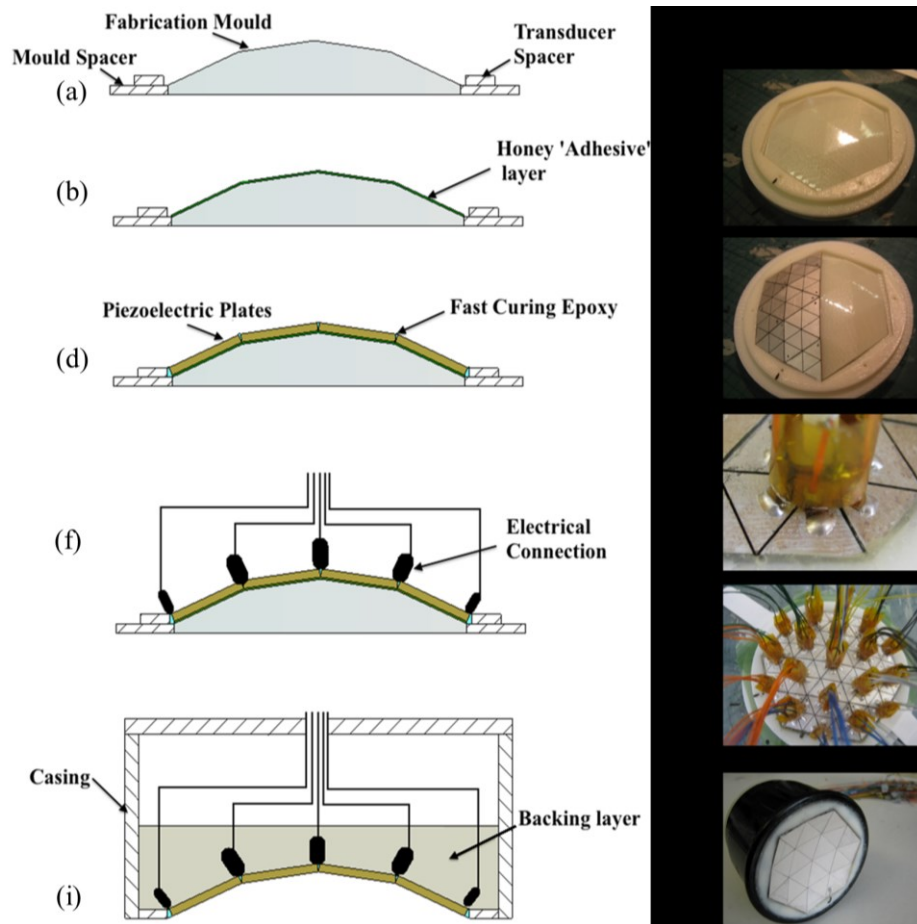
113 The process to assemble the array transducer from the machined triangular plates is illustrated in Fig. 2,
114 with a corresponding photograph for each step.

115 An important aspect of this process is the placement of each triangular plate in the position needed to
116 create the 3D faceted structure. The target wavelength, $\lambda \approx 1.5$ mm, indicates the need for precision much
117 better than 1 mm. Hence, an ABS thermoplastic mould with faceted surfaces matching the geodesic design
118 was made by 3D printing (uPrint SE 3D Printer, Stratasys Ltd, USA), as seen in Fig. 2a and 2c. The layer
119 resolution of the 3D printer was 0.254 mm. Honey thinned in a small container in a warm water bath at 50°C
120 was used to hold the plates in place, providing lower viscosity compared to other temporary adhesive options
121 such as silicon grease and thus minimizing the layer thickness on the mould (Fig. 2b). The use of honey also
122 allows the mould to be released and the residue to be removed with water. The triangular composite plates
123 were placed on the mould in the arrangement indicated in Fig. 1b and secured with 5 min-curing epoxy
124 (Araldite® Rapid, Huntsman Advanced Materials GmbH, Switzerland), (Fig.2d, e).

125 Because of the thermal sensitivity of PMN-PT piezocrystal, with rhombohedral to tetragonal phase
126 transition temperature, $T_{RT} \approx 80^\circ\text{C}$ [21], conductive silver epoxy (G3349, Agar Scientific, UK) rather than
127 soldering was used for the electric connections. Silver ink was also discarded as an option as its viscosity is
128 much lower than that of silver epoxy and it does not have the physical integrity to maintain its shape during
129 curing. Since this requires ~ 30 mins curing time at 55°C, custom-designed interconnect upstands, Fig. 2g,
130 were made to hold the cables in place during curing. These also allowed multiple connections to be made
131 together, increasing the assembly efficiency. Each upstand took the form of a hexahedron comprising two
132 plastic nuts stacked together (528-132, RS Components, Northants, UK). A flexible printed circuit board
133 (fPCB) made in house was attached around the hexahedron and alternate active and ground tracks were
134 connected to micro co-axial cables taken from commercial devices withdrawn from service (Toshiba Medical
135 Systems Europe, Zoetermeer, Netherlands). Each upstand supported six interconnects and the hexahedral
136 shape allowed fan-out of the active tracks to minimize the risk of shorting. Once each upstand had been

137 prepared, it was fixed to the back of the array element assembly with the 5 min-curing epoxy and the signal
 138 tracks were connected to the sub-diced triangular composites with conductive silver epoxy (Fig. 2f, g, and h).
 139 19 upstands were required for the array: 13 centrally with six micro co-axial cables each, and six at the
 140 perimeter of the array with three micro co-axial cables each. The array assembly was then transferred into a
 141 pre-heated oven to cure the conductive silver epoxy.

142 Integration with the outer casing followed. A mixture of micro-balloons (K1, 3M, USA) and epoxy
 143 (Epofix, Struers A/S, Ballerup, Denmark), mass ratio 1:2, was compressed carefully onto the back of the array
 144 element assembly between the interconnect upstands, to act as a mechanical support for the array but with
 145 reduced acoustic damping compared with unfilled epoxy because of the higher attenuation and lower acoustic
 146 impedance. These parameters cannot be quantified as it is impossible to achieve penetration of sound through
 147 the filled epoxy to measure them. After the backing layer was cured, the assembly was released from the
 148 mould and the casing was sealed with a watertight rear cover (Fig.2i, j). Finally, remaining honey was
 149 removed with warm water and a silver ink common ground was applied on the front face of the array.

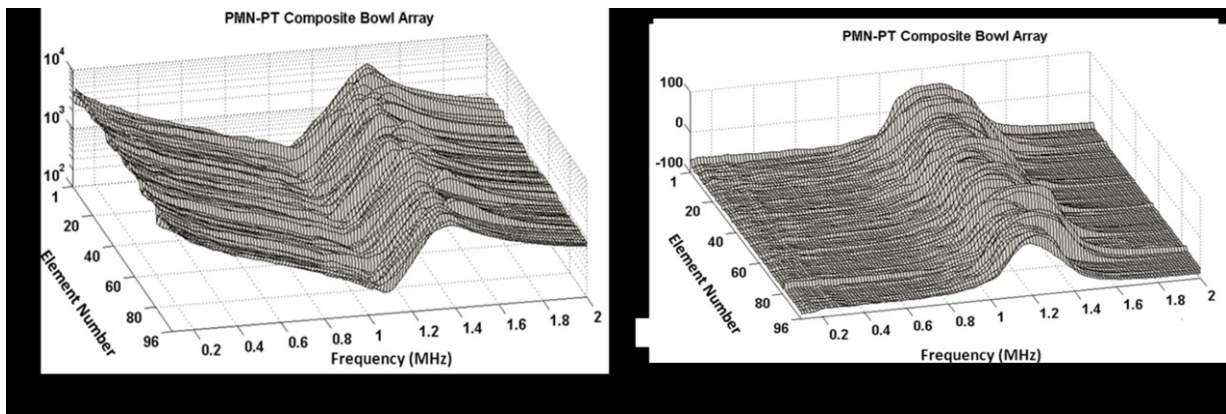


150
 151 *Figure 2. Assembly process for faceted bowl arrays: (a) mould with spacers, (b) with honey applied, (c) ready for the*
 152 *piezoelectric plates to be applied; (d) with the plates in place, (e) showing twelve plates, (f) electrical connections*
 153 *added at the plate vertices; (g) detail of the interconnect upstand scheme, (h) shown in overview, (i) with casing,*
 154 *backing layer and sealing plate added and (j) the complete array.*

155 5. Array Characterisation and Evaluation

156 5.1. Electrical Impedance Spectroscopy

157 The complex electrical impedance of each of the 96 elements of the piezocrystal composite array was
158 measured with an impedance analyzer (4395A, Agilent Technologies / Keysight, Santa Clara, CA, USA) with
159 the results plotted in Fig. 3. All 96 elements are fully functional without open or short connections. The
160 fundamental resonance and anti-resonance frequencies of the elements across the array, with standard
161 deviation, are $f_r = 1.05 \pm 0.02$ MHz and $f_a = 1.39 \pm 0.04$ MHz, respectively. The electrical impedance
162 magnitude $|Z| = 241 \pm 57 \Omega$ at the value of f_r for each element. The reasons for the large standard deviation are
163 three-fold: non-uniformity of piezocrystal material as purchased from two different production batches
164 (composite velocities measured to be 3285 m/s and 3490 m/s, respectively); variations in the individual
165 piezocrystal composite fabrication; and the systematic size differences between the triangular plates.

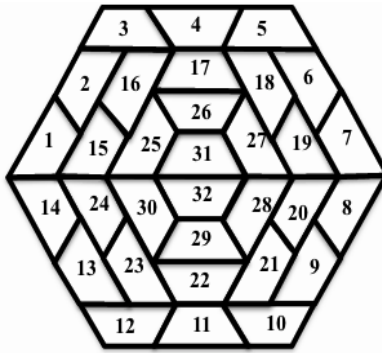


166

167 *Figure 3. Complex electrical impedance (a) magnitudes and (b) phases of all 96 elements of the piezocrystal composite*
168 *array*

169 5.2. Acoustic Pressure Field Mapping

170 The arrays were connected to commercial array control electronics (FI Toolbox DSL32T, Diagnostic
171 Sonar Ltd, Livingston, UK), customized to provide continuous wave output [22]. To match the 32
172 transmission channel count on the driving system, the 96 individual elements of the array were grouped into
173 32 channels, with sets of three adjacent elements connected together as shown in Fig. 4.

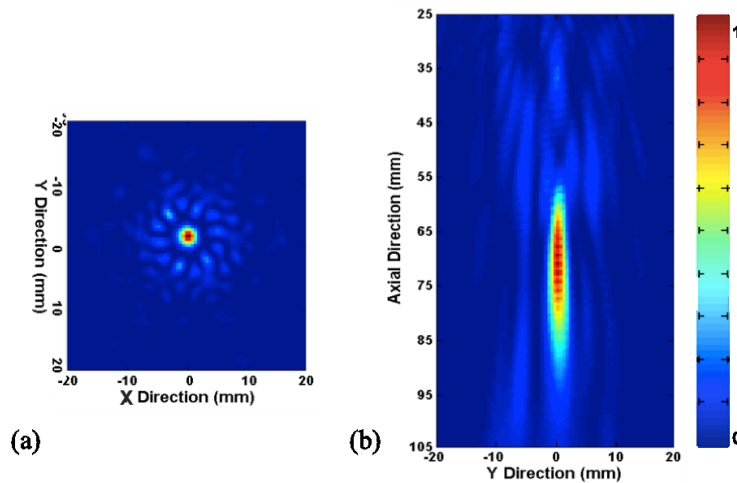


174

175 *Figure 4. Sketch of the distribution of 32 channels on the geodesic array in 2D segmented annular configuration*

176 *5.2.1 Natural focusing*

177 The focusing ability of the geodesic array configuration was tested initially with the bulk ceramic array,
 178 with its 32 groups of elements driven at 1.0 MHz, by mapping the beam profile over two perpendicular planes
 179 intersecting the transducer focus. To do this, the array was immersed in a tank of degassed water and a
 180 0.5 mm diameter needle hydrophone (Precision Acoustics Ltd, Dorchester, UK) was attached to a 3-axis
 181 motorized scanning system to measure the acoustic intensity at 0.5 mm increments. A natural focus was
 182 achieved with the geodesic structure, as shown in Fig. 5. The -3 dB (full width half maximum, FWHM) beam
 183 width at the focus was 2.4 mm and it was 21 mm in length. The intensities of all secondary side lobes were
 184 below -12 dB relative to the peak amplitude of the main lobe.



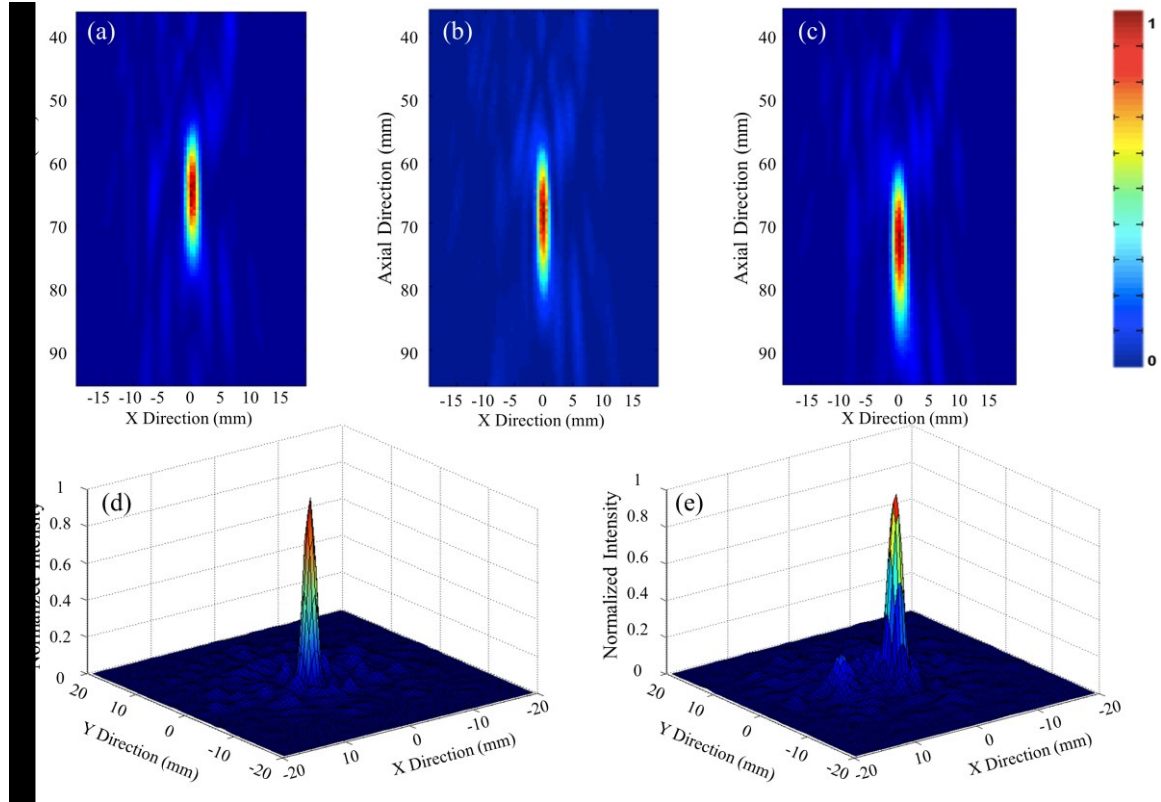
185

186 *Figure 5. Normalized output acoustic intensity of the piezoceramic array in its natural focal plane (a) cross section*
 187 *74.5 mm from the centre of the array and (b) axial scan.*

188 *5.2.2 Electronic focusing and steering*

189 The piezocrystal composite array was connected to array control system setup to enable programming of
 190 phase delays for steering and focusing. A phase quantisation step of 11.25° was possible, corresponding to a
 191 time delay of 31.2 ns at 1.0 MHz (time period 1.0 μ s). Phase correction of focusing aberrations based on
 192 hydrophone measurements was performed to allow for the increased non-uniformity of the piezocrystal

193 composite elements compared with the piezoceramic. The focus of the array was found at 69 mm in front of
 194 the array and it was then shifted and steered axially and laterally within a volume of $10 \times 5 \times 5 \text{ mm}^3$.
 195 Representative plots of the acoustic intensity fields are shown in Fig. 6. As an example, the -3 dB FWHM
 196 beam dimensions at the focus in Fig. 6b were 1.5 mm in width and 15 mm in length. The focusing gain of the
 197 array is 30, calculated from the square root of the ratio of the source area to the focal area. Similar to the
 198 results from the piezoceramic array, the intensities of the side lobes in the steered beam were below -12 dB
 199 compared to the main lobe.



201 *Figure 6. Normalized output acoustic intensity of the piezocrystal array with the focus set electronically to be*
 202 *(a) (0, 0, 64) mm, (b) (0, 0, 69) mm, (c) (0, 0, 74) mm, (d) (0, 0, 74) mm, and (e) (2.5, 0, 74) mm*

203 6. Discussion

204 Although the geodesic structure in this communication has been combined with the use of relaxor-based
 205 piezocrystals, it can be applied to any material, preferentially those in which natural crystal orientation exists,
 206 to form a self-focusing bowl resembling a section of a sphere. Gen. I piezocrystal, PMN-PT, was used here
 207 because of its commercial availability, but Gens. II and III piezocrystals will be worth investigating once the
 208 materials are available and their behavior is understood [23], not least as the issue of additional DC bias at
 209 high drive levels is moot for them [21].

210 The triangles used to form the proposed geodesic structure are not standard geometries available from
211 piezoelectric material suppliers but they can be prepared easily with a dicing saw. Besides the $6V$ icosahedron
212 dome structure implemented here, other geodesic dome structures exist, e.g. $4V$ and $5V$ [19] and could be
213 selected to match the aperture and focal length of a particular array design.

214 3D printing was integrated easily into our assembly process and has shown its potential to aid future
215 ultrasonic transducer development when complex geometrical configurations are needed. The maximum build
216 size of the printer may constrain the array size and aperture but the mould could be printed in several parts for
217 later assembly if a larger scale transducer is needed.

218 Electrical interconnects for multiple elements are a challenge during array assembly, especially with
219 complex shapes such as those discussed here. The interconnection upstands we used worked well with our
220 array and expedited the interconnect process. Although use of flexible PCBs from array to instrumentation
221 might further reduce the effort required for interconnection, this technique still does not offer sufficient length
222 of track and direct cabling is thus preferred.

223 In the preliminary results from electronic focusing and steering, the intensities of the side lobes steering
224 along the axis were as low as -12 dB compared to the main lobe, whilst a -9 dB side lobe was observed when
225 steering the focus off the axis. This increase in sidelobe level is predictable because lateral shifting of the
226 focus was constrained by the 32-channel configuration. Since the electronics are modular, additional channels
227 could be configured to connect all 96 elements of the array individually, improving the focusing quality and
228 steering range.

229 Defocusing and therefore the need for phase aberration correction are unavoidable because of residual
230 aberration from the array itself and from distortion in the medium during ultrasound propagation. Considering
231 only the device, we noted that aberration caused by assembly, associated with the accuracy of the 3D printed
232 mould, was secondary to that caused by non-uniform elements resulting from a combination of the
233 characteristics of the individual piezocrystal composites and the non-uniformity of the piezocrystal material
234 [12]. The hydrophone-based phase correction we adopted gave FWHM beam diameter of approximately one
235 wavelength, but the sidelobe level could be improved further by increasing the number of electronic channels.

236 7. Conclusions

237 This communication has proposed and evaluated a novel faceted array structure inspired by geodesic dome
238 architecture, allowing the adoption of high performance piezocrystal materials, such as PIN-PMN-PT and Mn-
239 doped PIN-PMN-PT piezocrystals, for focused ultrasound applications, since the crystal orientation in
240 crystalline materials prevents formation into a bowl shape in the same way as piezoceramics. The details of
241 assembly of a 96-element array have been described, based on PMN-PT piezocrystal – epoxy composite, with
242 bulk piezoceramic providing a reference device with which good focusing was achieved. Electronic focusing
243 was found to be necessary for the piezocrystal composite array, with satisfactory results achieved even though
244 groups of three elements were connected. The same technique also allows steering of the focus. The array has
245 not been tested at therapeutic levels because the PMN-PT single crystal material available for this work would
246 require an additional DC bias field of about 400V, which was not available for the present work. The
247 customized commercial electronics we used could however further extend the potential of the geodesic array
248 for focused ultrasound applications.

249 Acknowledgements

250 In this work, Dr. Zhen Qiu was supported by the Scottish Universities Physics Alliance. The authors also
251 thank Diagnostic Sonar Ltd for providing the driving system, and Mr. Graeme Casey, University of Glasgow,
252 and Dr. Jack Ng, Heriot-Watt University, for their assistance with this project.

253 References

- 254 [1] J. E. Kennedy, "High-intensity focused ultrasound in the treatment of solid tumours.," *Nature Review Cancer*, vol.
255 5, pp. 321-7, 2005.
- 256 [2] T. M. Allen, "Liposomes. Opportunities in drug delivery," *Drugs*, vol. 54 Suppl 4, pp. 8-14, 1997.
- 257 [3] H. M. Hertz, "Standing - wave acoustic trap for nonintrusive positioning of microparticles," *Journal of Applied*
258 *Physics*, vol. 78, pp. 4845-4849, 1995.
- 259 [4] D. R. Daum and K. Hynynen, "A 256-element ultrasonic phased array system for the treatment of large volumes
260 of deep seated tissue," *Ultrasonics, Ferroelectrics and Frequency Control, IEEE Transactions on*, vol. 46, pp.
261 1254-1268, 1999.
- 262 [5] E. S. Ebbini and C. A. Cain, "A spherical-section ultrasound phased array applicator for deep localized
263 hyperthermia," *Biomedical Engineering, IEEE Transactions on*, vol. 38, pp. 634-643, 1991.
- 264 [6] V. Auboiroux, E. Dumont, L. Petrusca, M. Viallon, and R. Salomir, "An MR-compliant phased-array HIFU
265 transducer with augmented steering range, dedicated to abdominal thermotherapy," *Physics in Medicine and*
266 *Biology*, vol. 56, pp. 3563-82, 2011.
- 267 [7] Y. Qiu, H. Wang, C. E. Demore, D. A. Hughes, P. Glynne-Jones, S. Gebhardt, *et al.*, "Acoustic devices for
268 particle and cell manipulation and sensing," *Sensors (Basel)*, vol. 14, pp. 14806-38, 2014.
- 269 [8] P. Sun, G. Wang, D. Wu, B. Zhu, C. Hu, C. Liu, *et al.*, "High Frequency PMN-PT 1-3 Composite Transducer for
270 Ultrasonic Imaging Application," *Ferroelectrics*, vol. 408, pp. 120-128, 2010.
- 271 [9] M. F. Wallace, H. Mulvana, P. Marin, K. Mayne, M. P. Walsh, R. Wright, *et al.*, "Parametric Array Design and
272 Characterisation for Underwater Sonar and Medical Strain Imaging Applications," in *Ultrasonics Symposium,*
273 *2007. IEEE, 2007*, pp. 305-308.
- 274 [10] Y. Chen, K.-H. Lam, D. Zhou, Q. Yue, Y. Yu, J. Wu, *et al.*, "High Performance Relaxor-Based Ferroelectric
275 Single Crystals for Ultrasonic Transducer Applications," *Sensors*, vol. 14, p. 13730, 2014.

- 276 [11] S. Zhang, S.-M. Lee, D.-H. Kim, H.-Y. Lee, and T. R. Shrout, "Elastic, Piezoelectric, and Dielectric Properties of
277 0.71Pb(Mg1/3Nb2/3)O3–0.29PbTiO3 Crystals Obtained by Solid-State Crystal Growth," *Journal of the American*
278 *Ceramic Society*, vol. 91, pp. 683-686, 2008.
- 279 [12] Z. Qiu, M. R. Sadiq, C. Demore, M. F. Parker, P. Marin, K. Mayne, *et al.*, "Characterization of piezocrystals for
280 practical configurations with temperature- and pressure-dependent electrical impedance spectroscopy,"
281 *Ultrasonics, Ferroelectrics and Frequency Control, IEEE Transactions on*, vol. 58, pp. 1793-1803, 2011.
- 282 [13] K. Yohan, A. D. Maxwell, T. L. Hall, X. Zhen, L. Kuang-Wei, and C. A. Cain, "Rapid prototyping fabrication of
283 focused ultrasound transducers," *Ultrasonics, Ferroelectrics, and Frequency Control, IEEE Transactions on*, vol.
284 61, pp. 1559-1574, 2014.
- 285 [14] B. I. Raju, C. S. Hall, and R. Seip, "Ultrasound therapy transducers with space-filling non-periodic arrays,"
286 *Ultrasonics, Ferroelectrics and Frequency Control, IEEE Transactions on*, vol. 58, pp. 944-954, 2011.
- 287 [15] Q. Zhou, X. Xu, E. J. Gottlieb, L. Sun, J. M. Cannata, H. Ameri, *et al.*, "PMN-PT single crystal, high-frequency
288 ultrasonic needle transducers for pulsed-wave Doppler application," *Ultrasonics, Ferroelectrics, and Frequency*
289 *Control, IEEE Transactions on*, vol. 54, pp. 668-675, 2007.
- 290 [16] K. H. Lam, Y. Chen, K. F. Cheung, and J. Y. Dai, "PMN–PT single crystal focusing transducer fabricated using a
291 mechanical dimpling technique," *Ultrasonics*, vol. 52, pp. 20-24, 1// 2012.
- 292 [17] W. A. Smith, "The role of piezocomposites in ultrasonic transducers," in *Ultrasonics Symposium, 1989.*
293 *Proceedings., IEEE 1989*, 1989, pp. 755-766 vol.2.
- 294 [18] G. Harvey, A. Gachagan, J. W. Mackersie, T. McCunnie, and R. Banks, "Flexible ultrasonic transducers
295 incorporating piezoelectric fibres," *Ultrasonics, Ferroelectrics, and Frequency Control, IEEE Transactions on*,
296 vol. 56, pp. 1999-2009, 2009.
- 297 [19] B. Carlo, "The Wooden Roofs of Leonardo and New Structural Research," *Nexus Network Journal: Architecture*
298 *and Mathematics*, vol. 10, pp. 27-38, 2008.
- 299 [20] A. L. Bernassau, D. Hutson, C. E. Demore, and S. Cochran, "Characterization of an epoxy filler for
300 piezocomposites compatible with microfabrication processes," *IEEE Trans Ultrason Ferroelectr Freq Control*,
301 vol. 58, pp. 2743-8, Dec 2011.
- 302 [21] S. Zhang and T. R. Shrout, "Relaxor-PT single crystals: observations and developments," *Ultrasonics,*
303 *Ferroelectrics and Frequency Control, IEEE Transactions on*, vol. 57, pp. 2138-2146, 2010.
- 304 [22] Z. Qiu, R. Habeshaw, S. Cochran, and L. Dave, "Customized modular multichannel electronics for ultrasound-
305 mediated targeted drug delivery with a geodesic piezocrystal phased array," in *Ultrasonics Symposium (IUS),*
306 *2014 IEEE International*, 2014, pp. 811-814.
- 307 [23] X. Liao, Z. Qiu, T. Jiang, M. Sadiq, Z. Huang, C. Demore, *et al.*, "Functional Piezocrystal Characterisation under
308 Varying Conditions," *Materials*, vol. 8, p. 5456, 2015.

309